In-Situ Observation of Solid Electrolyte Interphase Formation in Ordered Mesoporous Hard Carbon by Small-Angle Neutron Scattering

ARTICLE *in* THE JOURNAL OF PHYSICAL CHEMISTRY C · APRIL 2012

Impact Factor: 4.77 · DOI: 10.1021/jp3012393

5 AUTHORS, INCLUDING:

Craig A Bridges
Oak Ridge National Laboratory
78 PUBLICATIONS **1,114** CITATIONS

SEE PROFILE

Parans Paranthaman
Oak Ridge National Laboratory
444 PUBLICATIONS **9,722** CITATIONS

SEE PROFILE

Xiao-Guang Sun
Oak Ridge National Laboratory
69 PUBLICATIONS **1,293** CITATIONS

SEE PROFILE

THE JOURNAL OF PHYSICAL CHEMISTRY C

Article

pubs.acs.org/JPCC

In Situ Observation of Solid Electrolyte Interphase Formation in Ordered Mesoporous Hard Carbon by Small-Angle Neutron Scattering

Craig A. Bridges,*[,†] Xiao-Guang Sun,[†] Jinkui Zhao,[‡] M. Parans Paranthaman,[†] and Sheng Dai[†]

[†]Chemical Sciences Division, and [‡]Spallation Neutron Source, Oak Ridge National Laboratory, Oak Ridge, Tennessee 37831, United States

Supporting Information

ABSTRACT: The aim of this work was to better understand the electrochemical processes occurring during the cycling of a lithium half-cell based on ordered mesoporous hard carbon with time-resolved in situ small-angle neutron scattering (SANS). Utilizing electrolytes containing mixtures of deuterated (^{2}H) and nondeuterated (^{1}H) carbonates, we have addressed the challenging task of monitoring the formation and evolution of the solid−electrolyte interphase (SEI) layer. An evolution occurs in the SEI layer during discharge from a composition dominated by a higher scattering length density (SLD) lithium salt to a lower SLD lithium salt for the ethylene carbonate/dimethyl carbonate (EC/DMC) mixture employed. By comparing half-cells containing different solvent deuteration levels, we show that it is possible to observe both SEI formation and lithium intercalation occurring concurrently at the low voltage region in which lithium intercalates into the hard carbon. These results demonstrate that SANS can be employed to better understand complicated electrochemical processes occurring in rechargeable batteries, in a manner that simultaneously provides information on the composition and microstructure of the electrode.

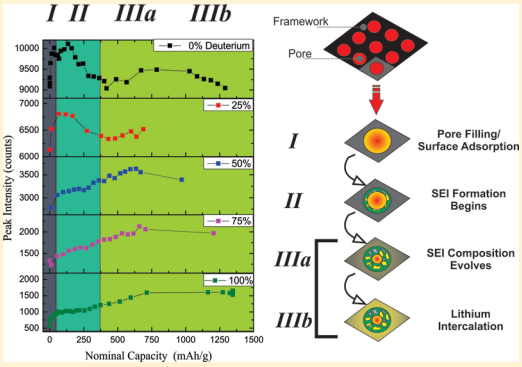

1. INTRODUCTION

Graphite has been used as a standard anode material in commercial lithium ion batteries (LIBs) because of its low cost, low lithium intercalation potential, and good cycling stability. However, its limited theoretical capacity of 372 mAh g^{-1} and poor rate performance have hindered its application in electric vehicles (EVs) and hybrid electric vehicles (HEVs). As an alternative to graphite, turbostratic carbons are promising candidates as anode materials in LIBs because of their high Li-storage capacity and good rate performance.[1] However, they usually suffer from the formation of a solid−electrolyte interphase (SEI), composed of electrolyte that has been reduced at reactive sites on the electrode surface, which can cause significant initial irreversible capacity loss and reduce battery life.[2,3] Reduction of the electrolyte to form a SEI is the result of a number of factors, though predominantly due to a larger surface area containing more reactive sites.[4] Hard carbons are another class of carbon anodes that have been found to be particularly advantageous in terms of high capacity and long cycle life, related to 3d highly porous and connected architectures,[5,6] though they may suffer from lower density and irreversible capacity issues.[4,5,7,8] Despite the importance of the SEI to battery performance, it remains a formidable challenge to observe the growth of this layer, and the mechanism of SEI formation in carbon anodes remains a key unsolved problem in battery research.[9]

Many ex situ studies have been performed to characterize the composition and structure of the SEI layer. These have typically focused on the use of surface analysis methods such as X-ray photoelectron spectroscopy (XPS), atomic force microscopy (AFM), and scanning tunneling microscopy (STM) or the use of vibrational spectroscopy such as FTIR or Raman.[10] While a great deal of understanding has been gained, it is difficult to avoid irreversible changes in the SEI layer when performing ex situ studies, necessitating rigorous experimental controls during washing and isolation of the electrode from the cycled cell. Furthermore, the details of how the SEI layer forms and evolves with cycling have been elusive. To obtain these details, it is necessary to examine the evolution of the SEI by using in situ techniques.

To understand the lithiation mechanism of carbon electrodes, studies have been performed on a variety of carbon anodes using in situ wide-angle X-ray scattering (WAXS), in situ small-angle X-ray scattering (SAXS), and ex situ small-angle neutron scattering (SANS).[1,11,12] The insertion of lithium has been observed by monitoring the changes in lattice parameter of carbon with WAXS and by the changes in electron density during discharge in the low potential region for SAXS.[12] However, X-ray techniques are relatively insensitive to changes

Received: February 7, 2012
Revised: March 12, 2012
Published: March 14, 2012

in lithium content due to the low scattering factor of lithium and are unable to observe the formation of the weakly scattering SEI layer. In addition, ex situ studies with SANS have been used to examine the electrode structure of disordered hard carbon, as lithium has a large scattering length in neutrons as compared with X-ray scattering.[11,13] These ex situ studies have shown that lithium inserts first into the periodically layered region, followed by insertion into interlayer nanovoids at the deep lithiation stage (low potential region).[11] While these approaches have been useful in understanding the lithiation of carbon at low potentials, they provide little information for the process of SEI formation. Other methods such as FTIR, XAS, and atomic force microscopy, among others, have also been adapted to in situ studies of rechargeable batteries;[14] while these methods are powerful, they do not provide the combination of microstructural and compositional information of in situ SANS.

We describe here the use of a high capacity and large surface-area ordered mesoporous carbon as a model cathode material for in situ electrochemical SANS studies, used in a half-cell configuration versus an isotopically enriched ^{7}Li anode. As a result of the large surface area of the carbon and small pore diameter of ~6 nm, the SEI layer becomes a significant fraction of the total pore scattering. To observe the decomposition of electrolyte, a standard ethylene carbonate/dimethyl carbonate (EC/DMC) composition has been chosen in which the carbon surface chemistry is dominated by EC reduction.[15] Solvent deuteration has been employed to modify the contrast of H/D containing species with the carbon framework. By this approach, SANS data have been used to directly observe the formation and evolution of the SEI layer, along with lithium intercalation and removal from the carbon framework.

2. EXPERIMENTAL SECTION

The ordered mesoporous carbon was synthesized as reported previously.[16,17] The carbon electrode was obtained by casting a well-homogenized slurry of ordered mesoporous carbon (80 wt %), carbon black (5 wt %), and PVdF (15 wt %) in the solvent *N*-methyl-2-pyrrolidone (NMP) on a copper foil with a doctor blade. After the solvent was evaporated, the electrodes were pressed under a hydrolytic pressure of 1 ton for 1 min before cutting into discs with areas of 1.327 cm^2 and further dried at 110 °C for 24 h before transferring into a glovebox for cell assembling. The typical loading of active material is about 4 mg. Coin cells of CR2032 were assembled by using lithium metal foil as anode, ordered mesoporous carbon as cathode, and commercial Celgard as separator. The electrolyte solutions consist of 1.0 M $LiPF_6$ in mixtures of nondeuterated EC/DMC solvent (weight ratio of 1:2) and deuterated solvent of dEC/dDMC (weight ratio of 1:2), to form a series of mixed deuterated/nondeuterated solutions with 0%, 25%, 50%, 75%, and 100% deuterated electrolyte. Deuterated electrolytes were purchased from Aldrich, with isotopic purities of 98 atom %D (dEC) and 99 atom %D (dDMC). The water content in nondeuterated electrolyte was below 10 ppm, whereas it was 50 ppm in the deuterated electrolyte. The cells assembled from different electrolyte solutions will be referred to in the text as nondeuterated (0%D), 25%D, 50%D, 75%D, and 100%D cells. To ensure minimal neutron absorption, isotopically enriched ^{7}Li metal was employed as the anode. The Li || Carbon cell was tested on a Land battery testing station under different current densities with cutoff voltages of 3−0.005 V at ambient temperature.

Small-angle neutron scattering (SANS) data were collected on the EQ-SANS instrument at the Spallation Neutron Source (SNS). The experiment used the sample to detector distance of 4 m and dual incident neutron wavelength bands of 2.5−6.1 Å and 9.4−13.4 Å by using the instrument's frame-skipping mode.[18] The covered neutron momentum transfer (Q) range lies between 0.006 and 0.3 Å^{-1}. The presented data correspond to ~20−60 min of data collection time per sample at the SNS power level of ~800 kW. Data reduction and analysis were performed with software developed at the EQ-SANS beamline.[19,20] Scattering length densities were calculated with the widely used NIST calculator (http://www.ncnr.nist.gov/resources/sldcalc.html), which computes the sum of all thermal neutron scattering length values from all nuclei within a unit sample volume. For all components, the SLD was calculated with density values obtained from available reference data, with the exception of the lithium methyl carbonate $(CH_2OCO_2Li)_2$ for which the density was estimated from closely related alkyl carbonate compounds (see Supporting Information). Representative examples of calculated scattering length densities are given in the Supporting Information (Table S1).

Specially constructed holders were used to locate the coin cells in the neutron beam and provide electrical contact for the initial discharge and subsequent charge cycles. A 9 mm diameter neutron aperture was used to locate the beam at the center of the coin cell. Due to activation in the neutron beam, coin cells could not be recovered for complete ex situ chemical analysis at the end of the experiment. Given the half-cell configuration used in these experiments, we define "discharge process" as lithium intercalation into the carbon electrode, "charge process" as lithium deintercalation from the carbon electrode, and "fresh cells" as cells that have been assembled but not yet discharged. The "reference cell" was designed to assist in isolating the signal from the carbon electrode in the SANS data and contains all the components of other coin cells (separator, electrolyte, spring, binder) except for the carbon electrode. The current used during the initial discharge process for the deuterated (100%D) and nondeuterated (0%D) cells was increased in increments as follows: 10, 50, 75, 100, 150, and 200 μA. Recharging for these cells was performed at a rate of 100 μA, followed by 150 μA. This procedure made a full cycle of discharge and charge possible within the time frame of the neutron experiment, while ensuring that data containing important details would not be missed during the initial stages of the experiment. Full details of the cycling procedures for all cells are given in the Supporting Information.

3. RESULTS AND DISCUSSION

Coin cells were discharged in situ on the EQ-SANS beamline, with SANS data collection at regular increments as shown in Figure 1(A) for the electrochemical profile of a cell containing deuterated ethylene carbonate (dEC) and deuterated dimethyl carbonate electrolyte (dDMC). The first discharge/charge cycle may be roughly divided into stages according to: (I) Initial discharge, (II) SEI formation, (III) lithium intercalation, and (IV) lithium removal (charging). This division may be justified on the basis of electrochemical data and SANS data and is applicable to all of the coin cells examined.

Before considering further the SANS data and its interpretation, it is useful to review some basic principles of small-angle neutron scattering. SANS is principally concerned with the difference in scattering length density (ΔSLD) between components within the sample. The intensities that

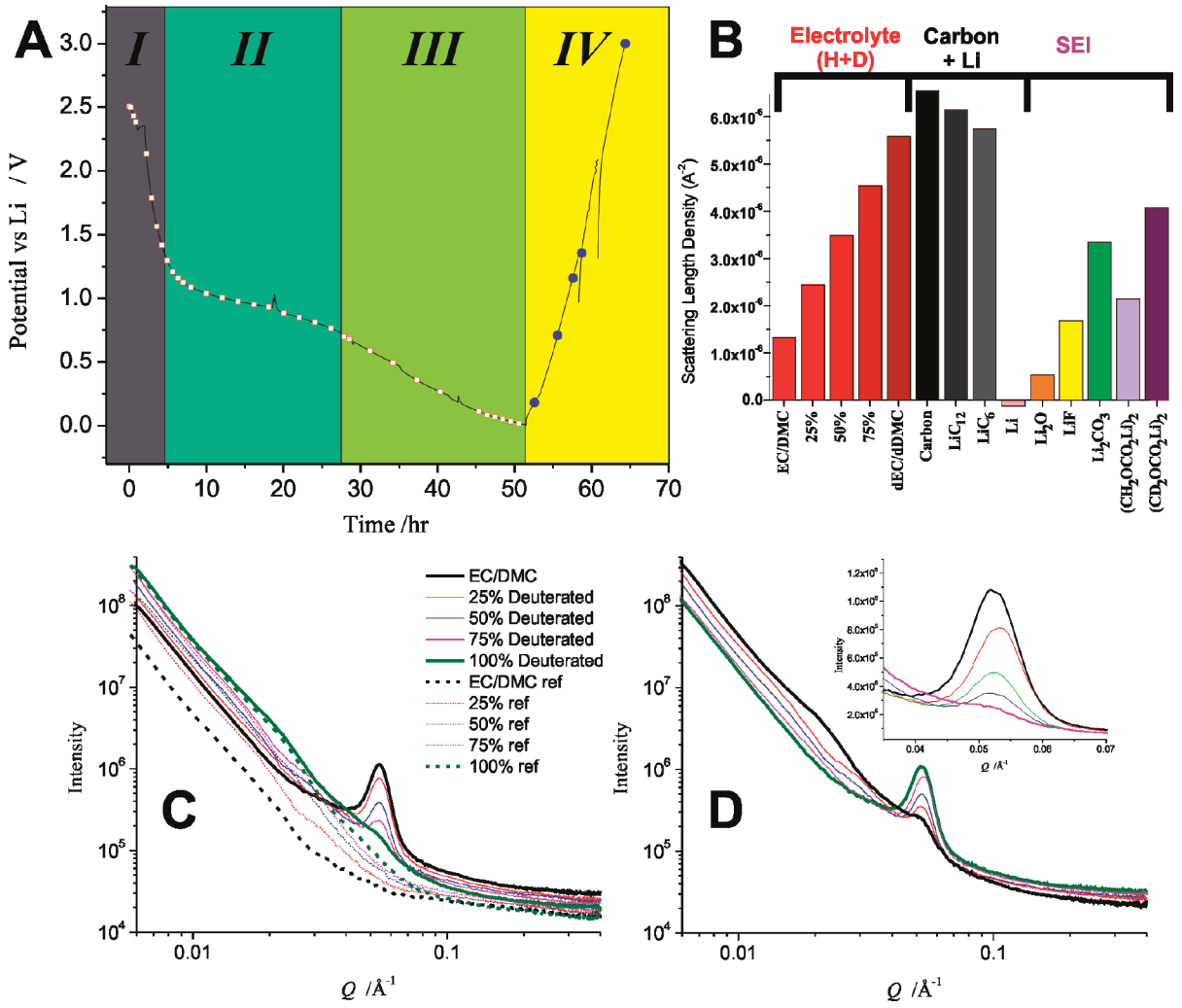

Figure 1. (A) Electrochemical profile for lithium insertion and removal from mesoporous hard carbon during an in situ SANS experiment. In panel (A) the profile for deuterated electrolyte (dEC/dDMC) is overlaid with regions to suggest the dominant electrochemical processes occurring at that time (stages I, II, III, and IV), as described in the text. Each point on plot (A) represent a SANS data set (averaged typically over 30 min−1 h data collection) during discharging (red square) and charging (blue circles). In (B), the variations in scattering length density for dominant components in the cathode are shown. The raw data for each electrolyte deuteration level are shown for the fresh cells in (C) and discharged cells in (D), with the reference cells for each electrolyte shown in (C). The mixing of dEC/dDMC and nondeuterated (EC/DMC) solvent provided a range of scattering contrast between the pores and the carbon framework, resulting in a trend from strong contrast for the nondeuterated cell to weak contrast for the deuterated cell.

are measured in a SANS experiment are proportional to the square of the difference in SLD (ΔSLD^2), which is termed the contrast. The SLD of a component is a function of its density and scattering length, and the scattering length of a component is a function of the elements present and their ratios. For example, the calculated SLD of the carbon framework is 6.65×10^{-6} Å^{-2} at a density of 2.0 g/mL; ethylene carbonate is 2.02×10^{-6} Å^{-2} at a density of 1.321 g/mL; while that of deuterated ethylene carbonate is 5.78×10^{-6} Å^{-2} at a density of 1.38 g/mL. The scattering length of H is negative, while that of D is positive, such that the deuteration of ethylene carbonate leads to a large increase in scattering length for the solvent. The difference in SLD between the carbon and the electrolytes provides a contrast. For battery electrodes studied here, the critical information is provided by the contrast between the carbon framework and the ∼6 nm pores. In this work, we consider how changes in the contrast between pore and framework are correlated with electrode chemistry during battery cycling.

To better understand the electrochemical processes occurring during each stage, we have prepared a series of cells containing different levels of solvent deuteration. The change in scattering length density is plotted in Figure 1(B) for a number of phases that may contribute to the contrast (ΔSLD) between the pore and framework in the cathode. A range of SLDs are presented for previously reported components of the SEI layer (e.g., LiF, Li_2CO_3). Any H/D containing component is expected to show a linear increase in SLD with deuteration level of the solvent, as in the case of the lithium alkyl carbonate $(CH_2OCO_2Li)_2$ in Figure 1(B). Note that the PVdF binder used in the carbon electrode has a calculated SLD similar to that of a ∼35%D electrolyte formulation ($\sim 2.9 \times 10^{-6}$ Å^{-2}), and as it does not play a direct role in the electrochemical processes and is primarily on the surface of the carbon electrode particles, it will be ignored in the following analysis. In terms of the framework, during the discharge process the SLD of the carbon decreases due to insertion of $^7Li^+$, as lithium has a negative scattering length. By comparing the calculated

dx.doi.org/10.1021/jp3012393 | J. Phys. Chem. C 2012, 116, 7701−7711

SLD for the framework and for each component in the pore with the observed data at each stage in the in situ discharge/charge cycle, we derive information about the chemical processes occurring in the pore.

The SANS data for fresh (Figure 1(C)) and discharge (Figure 1(D)) cells demonstrate the impact of variation in contrast between the pores and carbon framework. The largest contrast is observed for the pure nondeuterated ethylene carbonate (EC) and nondeuterated dimethyl carbonate (DMC) solvent mixture, resulting in a large peak near $Q \sim 0.054$ Å^{-1} that corresponds to the ordered pore−pore spacing of ∼116 Å. The observation of a large peak is consistent with the expectations of Figure 1(B), in which the dEC/dDMC mixture has a SLD nearly equivalent to the carbon framework, producing only a very weak peak relating to the ordering of the pores. A quantitative comparison is made in Table 1 of the calculated intensity ratios for various deuteration levels (I_c) with the observed intensity ratios (I_o) for cells prior to discharge. As the intensity of the peak is proportional to the square of the difference in SLD (ΔSLD^2) between the pore and framework, the ratio of this quantity for different deuteration levels should be consistent with the differences in observed intensities. The expected ratios are confirmed by the results in Table 1, which provides confidence in the calculated SLD values of the components in Figure 1(B).

Table 1. Calculated Peak Intensity (I_c) Ratios for Fresh Cells Compared with Observed Peak Intensity (I_o) Ratios

sample (x% D)	SLD (Å^{-2})	$I_{c(0\%D)}/I_{c(x\%D)}$	peak intensity (I_o)	$I_{o(0\%D)}/I_{o(x\%D)}$
0	1.39e^{-6}	1.00	9290(60)	1.00
25	2.45e^{-6}	0.64	6130(45)	0.66
50	3.50e^{-6}	0.36	2780(30)	0.30
75	4.56e^{-6}	0.16	1330(30)	0.14
100	5.61e^{-6}	0.04	570(50)	0.06

The raw in situ SANS data near the peak due to pore ordering are shown for all cells in Figure 2. An example of fitted data for the nondeuterated cell is given in the Supporting Information (Figure S1). The in situ data were fitted by using a combination of four functions: (1) fractal, (2) Debye−Bueche (DAB), (3) Gaussian, and (4) flat background (Figure S1, Supporting Information).

$$I(Q) = I_F Q^{-p} + \frac{I_{DAB}}{[1 + (AQ)^2]^2} + G_0\left[\frac{0.398}{s} e^{-1/2\left(\frac{Q-k}{s}\right)^2}\right] + B \quad (1)$$

The first term obeys the Porod law which describes the fractal scattering from the carbon material and the casing materials for the battery cell.[21] The variation in background at low Q with solvent is due to changes in contrast between the separator and electrolyte. The second term is the DAB term,[22,23] which describes the scattering from the pore surface. The third term is a Gaussian function that we use to model the diffraction resulting from the long-range pore−pore ordering, and the fourth term is a background. The backgrounds in these experiments arise primarily from the scattering of the battery electrolyte and are treated as flat across different Q-values for simplicity. There are no contributions in the reference cells to the peak of interest near $Q \sim 0.054$ Å^{-1}, and subtraction of the reference cell from the full cell shifted the background without affecting changes in relative intensity or peak position. Therefore, final fitting of the data was carried out against the raw data. In the current study, we focus our attention on the Gaussian peak, which displays clear trends with respect to deuteration level and state of charge; the DAB term is found to be relatively weak and less reliable. The Gaussian peak intensity relates to the scattering contrast between the pore and carbon framework, while the peak position is defined by the average pore−pore spacing. The results of the Gaussian fits are shown in Figure 3(A) and 3(B) for the peak intensity and peak position versus nominal specific capacity. These data are particularly rich with information relating to the electrochemical processes occurring at each stage during cell cycling.

Stage I: Initial Stage of Discharge. The first stage in the discharge of a fresh in situ cell occurs from the initial open cell voltage (OCV), typically near 2.5 V, to the lower voltage near 1.3 V, which is the onset reduction voltage of carbonate electrolytes.[24] This stage is shown as a purple band in Figure 1A and Figure 3, covering nominal capacity range from ∼0 to 372 mAh g^{-1}. The voltage profile in this range follows a robust trend that overlaps over many cycles, irrespective of whether SEI formation has completed, and thus represents a reversible electrochemical process rather than irreversible electrolyte decomposition. Different models of SEI formation below ∼1.3 V have considered that (1) the electrolyte may be reduced directly to form the SEI layer or (2) the solvent may partially cointercalate with lithium between graphene layers to form a ternary graphite intercalation compound (GIC) before decomposing into a SEI layer.[25,26] By examining the change in contrast between the framework and pore in the SANS data, we may consider what reversible electrochemical process provides the initial capacity and whether cointercalation of solvent happens before solvent reduction.

In all coin cells, the intensity and position of the Gaussian peak change rapidly during this initial discharge stage. The shift in peak position to lower Q corresponds to an increase in the pore−pore separation of ∼1 Å for all cells. The main influence on pore−pore separation is expected to be intercalation into the carbon framework. Significant intercalation of Li$^+$ cations is not expected until the lower voltage range (Stage III).[11] However, partial cointercalation of lithium and solvent may occur before SEI formation, and this remains as a possible explanation of the increase in pore−pore separation.

In conjunction with the shift in peak position, there is an increase in peak intensity, indicating an increase in contrast between the pores and carbon framework. The increase in contrast may arise from an increase in the SLD of the framework, a decrease in the SLD of the ∼6 nm pores, or both. An increase in the SLD of the framework could result from a large increase in the framework density, which is highly unlikely during a volume increase in the low capacity region. Furthermore, given the relatively low SLD of the solvent and the negative scattering length of lithium, it is expected that cointercalation of lithium and solvent should result in a decrease in the SLD of the framework and the peak intensity. Similarly, intercalation of Li$^+$ without solvent should result in a decrease in peak intensity if it occurs throughout the bulk. The most likely explanation for the increase in peak intensity is a decrease in the SLD of the ∼6 nm pores, which can be

dx.doi.org/10.1021/jp3012393 | J. Phys. Chem. C 2012, 116, 7701−7711

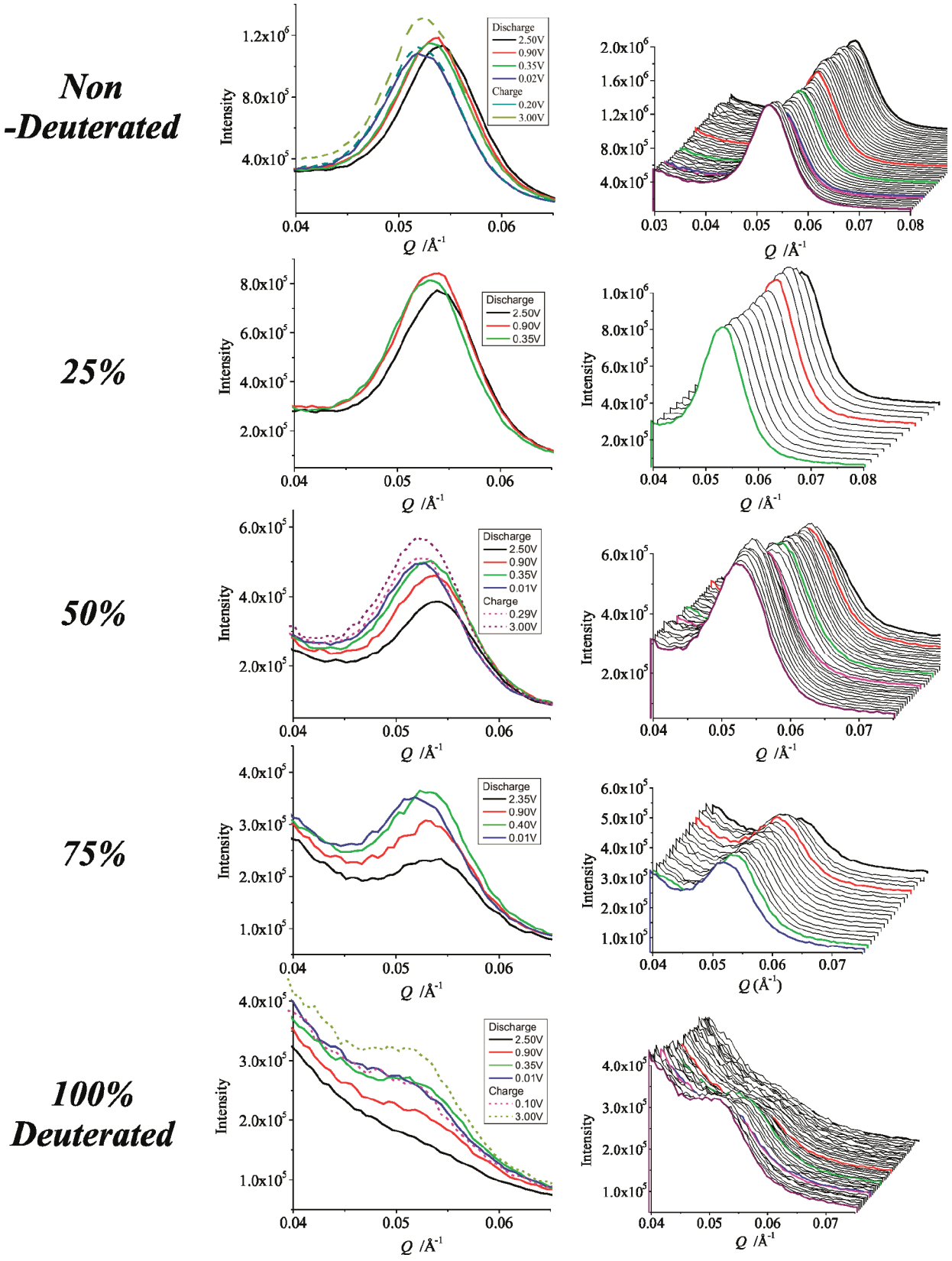

Figure 2. In situ SANS data for cycling of half-cells containing ordered mesoporous hard carbon cathodes, ^{7}Li anodes, and 1.0 M $LiPF_6$/EC/DMC electrolyte. The peak near $Q \approx 0.054$ Å^{-1} results from the ordering of the hard carbon pores (~116 Å pore−pore spacing). Significant changes in peak intensity and position are clearly evident during in situ discharge and charge of all cells. Data at selected voltages are shown on the left, and full sets of data are shown on the right. The data are presented with the fresh cell (initial state) starting in the back of the figure.

dx.doi.org/10.1021/jp3012393 | J. Phys. Chem. C 2012, 116, 7701−7711

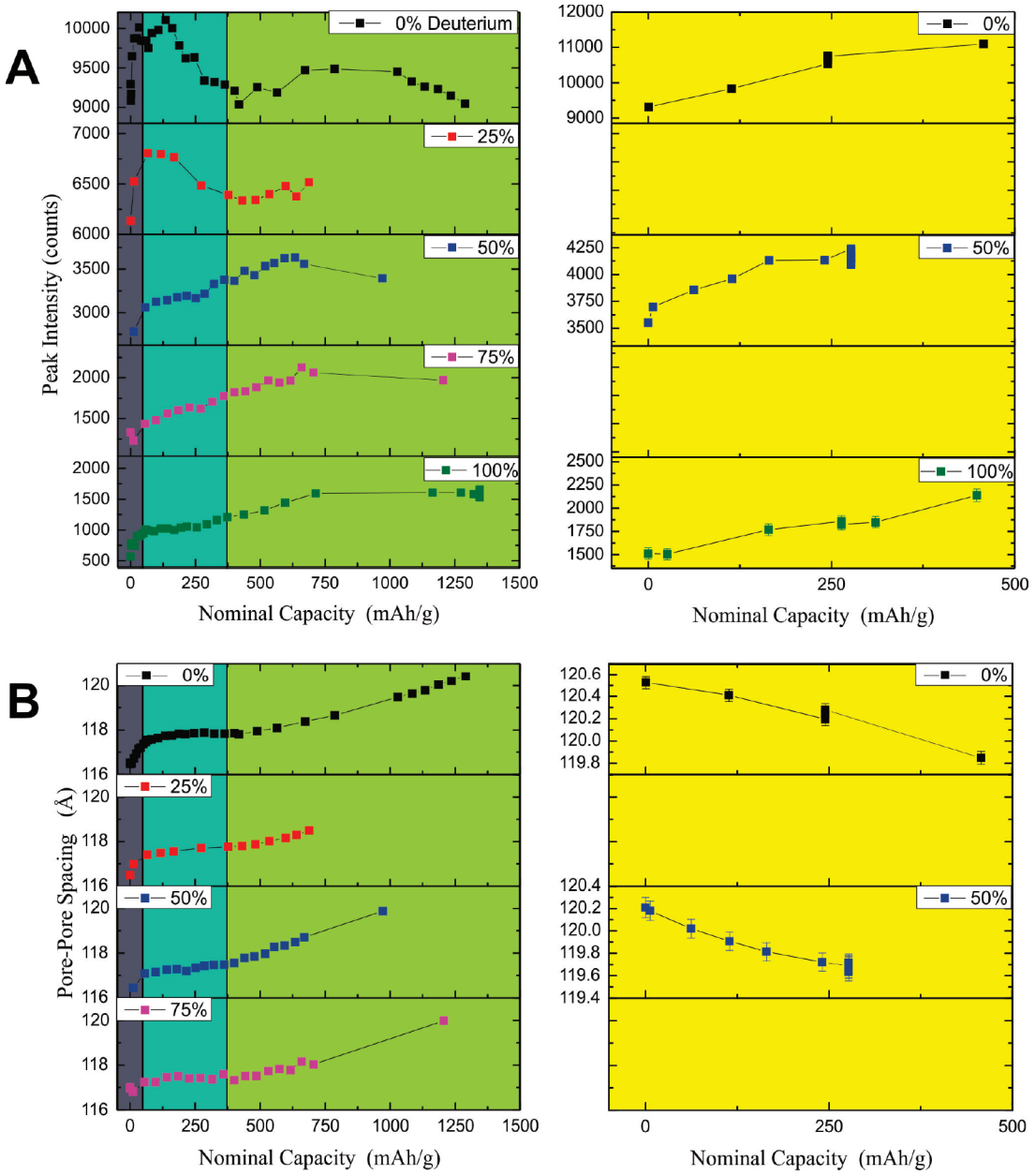

Figure 3. Results of fits to in situ SANS data derived from the Gaussian peak. The peak intensity versus nominal capacity is shown in (A), and the pore−pore spacing versus nominal capacity is shown in (B). The discharge process is given on the left and charge process on the right, while background colors indicate stages I (purple; initial discharge; 2.5−1.3 V), II (blue; SEI formation; 1.3−0.7 V), III (green; lithium intercalation; 0.7 V−5 mV), and IV (yellow; charging; 5 mV−3 V) of the initial charge/discharge cycle with a color scheme identical to Figure 1(A). These stages are defined in greater detail in the text. The terms discharging and charging are defined relative to the half-cell configuration in which carbon is the cathode. Errors derived from the fit are included and are typically smaller than the size of the data symbol.

explained by an increase in the concentration of lithium in the pores and on the framework surface.

When considering the change in position and intensity of the Gaussian peak, it is necessary to reconcile the possible cointercalation of lithium and solvent and increase in lithium concentration in the pore. It has been shown that the rate-determining step in Li^+ intercalation into the graphene layers is the process of stripping the solvation shell.[27] Therefore, when cointercalation of lithium and solvent begins, the process of solvent stripping may result in a lithium-rich layer near the surface of the framework. Models of lithium intercalation into the graphene layers at low temperature suggest that islands of lithium-rich compositions can form near the layer edge before migration further into the layers.[28] It is therefore likely that the scattering at this stage is dominated by an increased concentration of solvated lithium near the surface of the ~6 nm pores (adsorbed) and the intercalation of solvated lithium near the carbon surface followed by solvent stripping. The intensity change in the peak is visible due to the high surface area of the mesoporous carbon. The increased concentration of lithium with solvation shells near the surface could set the stage for SEI formation at lower voltages. Further work is necessary to confirm this model as appropriately describing the origin of the increase in peak intensity and pore−pore separation in Stage I.

Stage II: SEI Formation. The second stage in the discharge of a fresh in situ cell corresponds to the region of slowly varying

dx.doi.org/10.1021/jp3012393 | J. Phys. Chem. C 2012, 116, 7701−7711

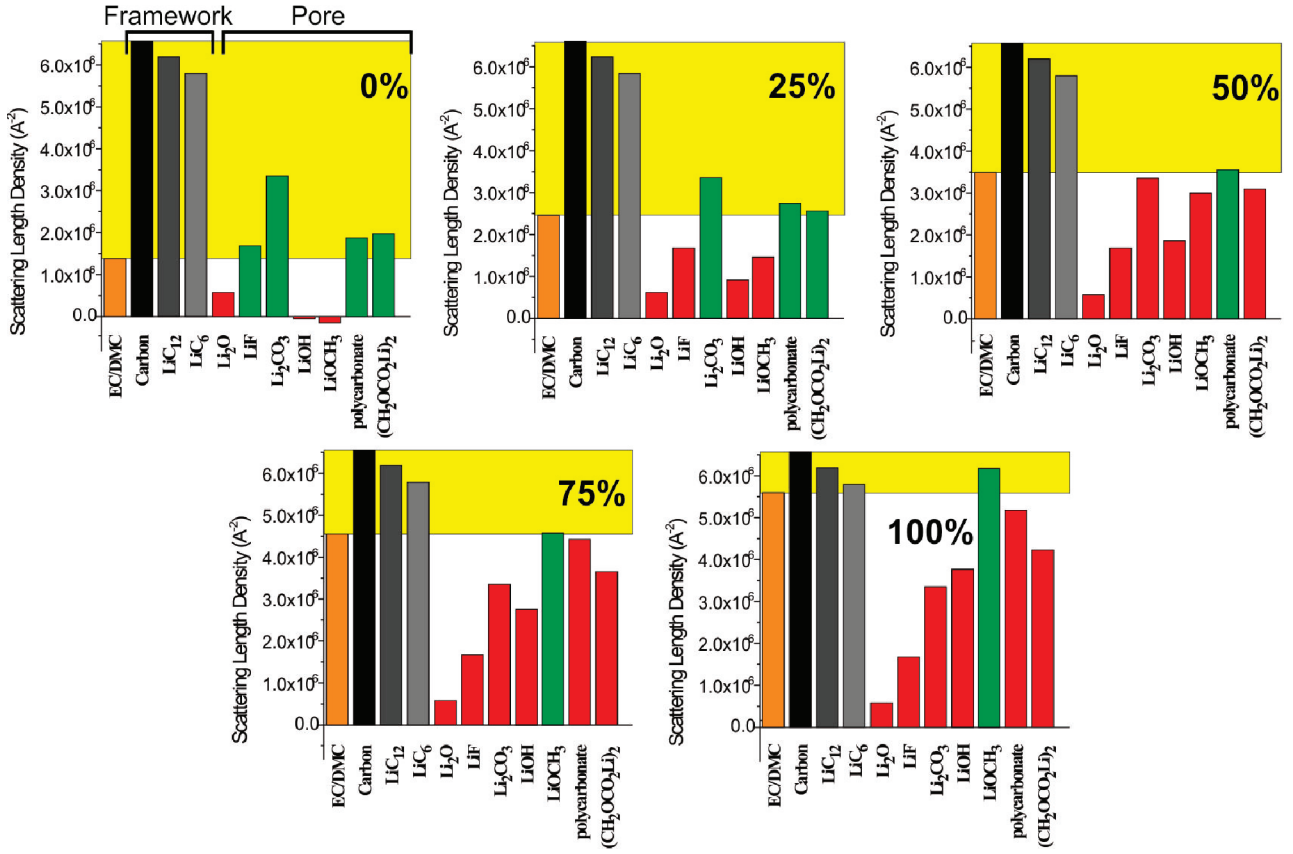

Figure 4. Plots comparing the calculated scattering length densities (SLDs) of the electrolytes, carbon framework, and potential components of the solid−electrolyte interphase (SEI) layer as a function of deuteration level. The deuteration level of the electrolytes varies from 0% to 100%, and the SLDs of the SEI layer have been adjusted accordingly for each case. The yellow band indicates the region over which a component in the SEI will result in a decrease in contrast between the framework and pore relative to a fresh cell, and these components have been highlighted in green for each deuteration level. Only the Li_2O and LiOH components will cause an increase in contrast for all deuteration levels.

voltage in the electrochemical profile (blue band in Figure 1(A) and Figure 3). A gradual decrease in the voltage is observed, resulting in a voltage range of ∼1.3 to ∼0.7 V over a nominal capacity range of 75 to 372 mAh g^{-1}. In this stage, the primary process occurring is thought to be the formation of the SEI layer, which is composed primarily of lithium salts.[24] As the consumption of lithium for SEI formation does not contribute to reversible capacity, the term "nominal" capacity is used to identify stages in the initial charge/discharge cycle. The impact of varying the deuteration level of the electrolyte in this region is striking, as the trend in peak intensity variation versus state of charge is not uniform for all electrolyte compositions (Figure 3(A)). The nondeuterated and 25%D cells display a maximum in peak intensity, followed by a decrease over the nominal capacity region from 150 to 372 mAh g^{-1}. Over this same region, the 50%D, 75%D, and 100%D cells show an increase in contrast (increase in peak intensity).

These results may be explained by the formation of a SEI layer with possible components including Li_2CO_3, alkyl lithium compounds such as $(CH_2OCO_2Li)_2$, LiF, Li_2O, and LiOH, or polycarbonates.[10] The exact composition of the SEI layer is not well-defined in the literature for a given cell chemistry (e.g., 1.0 M $LiPF_6$/EC/DMC), as it varies with the procedures and environments used in the electrode and cell preparation, as well as the water content in the cell components. Relative to the initial contrast window provided by the framework and electrolyte, the SLDs of possible SEI components vary greatly with deuteration level. We do not attempt to quantitatively specify particular compositions of the SEI, involving various combinations of possible components. This discussion will focus on what SEI components are consistent with the observed trends in Gaussian peak intensity with state-of-charge. For example, if the peak intensity decreases during SEI formation in the pore, it is not possible for the dominant component of the SEI to be a compound that would result in a peak increase.

The calculated SLDs for each of these components corrected for deuteration level are shown in Figure 4 for all cells and provide a useful basis for understanding the trends in peak intensity. For example, the formation of $(CH_2OCO_2Li)_2$ in the SEI should cause a decrease in contrast for the 0−25% deuteration levels, as its SLD is between the SLD of EC/DMC and carbon (green color, as it is within the yellow bands in Figure 4). At the 50% deuteration level and above, $(CH_2OCO_2Li)_2$ in the SEI should cause an increase in contrast (red color, as it is below the yellow bands in Figure 4). LiF increases peak intensity at 25%D and above, while Li_2CO_3 increases peak intensity above 50%D. The lithium salts, Li_2O and LiOH, will cause an increase in contrast for all deuteration levels. The alkoxide $LiOCH_3$ should cause an increase in intensity from 0% to 50% deuteration levels, followed by a decrease in peak intensity at 75% and 100% deuteration levels. By examining these trends, it is possible to consider the possible dominant contributions to the SEI.

The trend in Gaussian peak intensity versus charge during SEI formation in Stage II is summarized in Table 2 for each

dx.doi.org/10.1021/jp3012393 | J. Phys. Chem. C 2012, 116, 7701−7711

Table 2. Possible SEI Components Responsible for Trend in Peak Intensity (Contrast) During Stage II

sample (% D)	trend in contrast	possible SEI components consistent with trend
0	decreasing	Li_2CO_3, $(CH_2OCO_2Li)_2$, LiF, polycarbonate
25	decreasing	Li_2CO_3, $(CH_2OCO_2Li)_2$, polycarbonate
50	increasing	Li_2CO_3, $(CH_2OCO_2Li)_2$, Li_2O, LiOH, LiF, $LiOCH_3$
75	increasing	Li_2CO_3, $(CH_2OCO_2Li)_2$, Li_2O, LiOH, LiF
100	increasing	Li_2CO_3, $(CH_2OCO_2Li)_2$, Li_2O, LiOH, LiF

deuteration level (%D). For each deuterated cell, possible SEI components are listed that could be responsible for the observed trend. Only the Li_2CO_3 and $(CH_2OCO_2Li)_2$ components can explain the change from decreasing to increasing the contrast between the framework and pore that occurs at the 50% deuteration level. For an EC-based solution, it is expected that $(CH_2OCO_2Li)_2$ and Li_2CO_3 are dominant reduction products. The formation of Li_2CO_3 from lithium alkyl carbonates is expected to occur more readily at elevated temperatures (~60 to 100 °C)[10] and at lower EC concentration in the solvent.[10,15] In addition, the presence of water is expected to promote the reaction to form Li_2CO_3 from $(CH_2OCO_2Li)_2$. Only these two SEI components, $(CH_2OCO_2Li)_2$ and Li_2CO_3, are present in all rows of Table 2. Assuming the composition of the SEI is the same for all cells, this would indicate that one (or both) is the dominant component of the SEI. However, Li_2O or LiOH may also form in the presence of water and LiF in the presence of HF. Given that the deuterated solvent mixture has a higher moisture content than the nondeuterated solvent mixture, it is possible that Li_2O, LiOH, or LiF could be increasingly present in the SEI with increasing deuteration level. If the composition of the SEI changes in this manner with increasing solvent deuteration, this could contribute to the change in trend observed in Table 2 at the 50% deuteration level.

An alternative explanation for the variation in contrast observed in Stage II, which may be readily discounted, is that insertion of lithium into the carbon framework is solely responsible. Insertion of lithium into the carbon framework will cause a decrease in contrast for the nondeuterated and 25%D cells, in agreement with the observed data over this voltage region. However, according to Figure 4 the change in SLD of carbon with increasing Li content should also cause a decrease in the contrast for the 50%D, 75%D, and 100%D samples, in disagreement with the observed trend. As demonstrated in Table 1, the calculated SLDs for fresh cells are in good agreement with the experimental results, proving that while it may contribute to the change in contrast at this stage lithium insertion cannot be responsible for the observed trends. Furthermore, very little shift in the Gaussian peak position is observed during Stage II (Figure 3(B)), while lithium insertion should cause an increase in the pore−pore separation. Note that for this high surface area (~600 m^2/g) mesoporous carbon cathode, a calculation assuming a constant 5.8 nm pore diameter suggests that formation of a dense ~1 nm SEI layer (reducing the pore diameter to 3.8 nm) would result in ~70% filling of the pores. The large volume fraction of the SEI layer makes its observation experimentally feasible. The only explanation consistent with the data is that the formation of the SEI layer is being observed.

Though it is expected that a number of these components are simultaneously present, only the $(CH_2OCO_2Li)_2$ and Li_2CO_3 components are consistent with all of the observed trends for Stage II; this indicates that one (or both) of these compounds is the dominant component at this stage, in agreement with the expectations for an EC-based solvent.

Stage III: Lithium Intercalation and Change in SEI Composition. The start of Stage III (green band in Figure 1(A) and Figure 3) is indicated by the accelerating decrease in the voltage below ~0.7 V due to the onset of significant lithium intercalation into the carbon and continues until the cell is fully discharged to 0.005 V. Furthermore, the increase in pore−pore separation provides further evidence that the onset of significant lithium intercalation into the framework begins below ~0.7 V.

Remarkably, at the beginning of Stage III all of the cells experience an increase in contrast versus state-of-charge (above 372 mAh g^{-1}), requiring a reversal in the trend for the nondeuterated and 25%D cells from Stage II. It is important to note that a simple change in the thickness of the SEI layer would not change the trend in contrast with state-of-charge. Given that according to the SLD calculations summarized in Figure 4 lithium insertion into carbon should result in a decrease in contrast for all cells, this implies that *a change in the chemistry of the SEI layer is occurring, which is observed during lithium insertion into carbon.* In Stage IIIa (Figure 5), a change in chemistry of the pore dominates the scattering, though in this region there is clearly lithium insertion into the framework. It has been reported in the literature that the SEI layer is not constant with cycling.[10] The change in trend of peak intensity from Stage II to Stage IIIa provides direct evidence for a change in the composition of the SEI layer during the initial discharge cycle.

To better clarify the evidence for a composition change in the SEI layer, we consider that the increase in contrast at the beginning of Stage III for all cells may be related to an increase in the SLD of the framework or a decrease in the SLD of the pore or a net increase in contrast arising from a change in both. Given the increase in volume, combined with intercalation of lithium (which has a negative scattering length), it is highly unlikely that there is an increase in SLD of the framework as this would require a large increase in framework density. Quantitatively, lithium intercalation into the carbon to form LiC_6 without changing the framework density is calculated to result in a decrease in peak intensity for the nondeuterated cell to ~70% of initial intensity, assuming that no change in the SLD of the pore occurs. For the other cells which contain deuterated electrolyte, due to the smaller contrast between the deuterated electrolyte with the framework, there should be a much larger percentage decrease in peak intensity with lithium insertion. However, the peak intensities actually increase in Stage IIIa, before eventually beginning to decrease near the end of the discharge cycle for each cell as lithium insertion dominates the scattering (Stage IIIb). In the lower voltage region, further lithium intercalation into interlayer nanovoids is used to explain the large lithium storage capacity of mesoporous hard carbons (up to ~1000 mAh/g), which should contribute to the observed decrease in peak intensity.[8,29−33] Despite the decrease in peak intensity in Stage IIIb, none of the fully discharged cells have peak intensities lower than their initial values as fresh cells (beginning of Stage I). The peak intensity is dependent upon the difference in SLD between the pore and framework. Therefore, despite a decrease in the SLD of the framework (relative to the fresh cell) arising from lithium intercalation,

dx.doi.org/10.1021/jp3012393 | J. Phys. Chem. C 2012, 116, 7701−7711

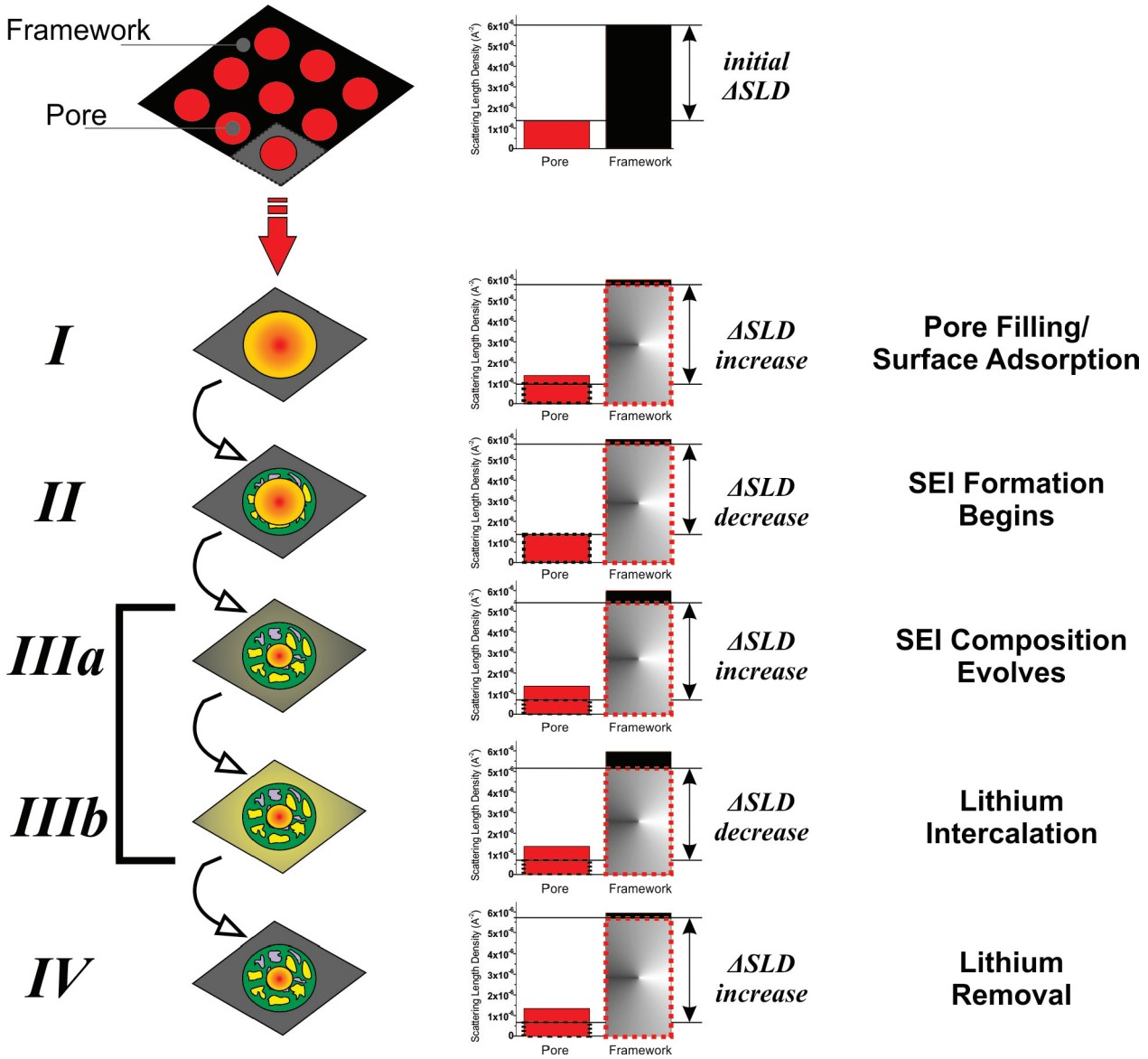

Figure 5. Schematic illustration of the various stages of the initial charge/discharge cycle for the nondeuterated cell, including: Stage I (pore filling and surface adsorption of solvated lithium during discharge), Stage II (SEI formation), Stage III (lithium intercalation), and Stage IV (lithium removal during charging). Changes in contrast (ΔSLD) consistent with the observed peak intensity data for each stage are shown in the middle. At each stage the *dominant* process affecting contrast is illustrated. In Stage IIIa, the evolution of the SEI to include more low SLD lithium salts is the dominant scattering process, while in Stage IIIb (at lower voltage) the lithium intercalation has the greatest impact on the contrast.

there is an even greater decrease in the SLD of the pore. In summary, lithium intercalation at the beginning of Stage III should result in a decrease in the contrast, rather than the increase observed for all cells. As a result, the trend in Stage IIIa for the nondeuterated and 25%D cells, which reverses their trend from Stage II, must be predominantly caused by a decrease in the SLD of the pore.

It has been reported that the chemistry of the SEI layer may change during cycling or storage.[34] This change may involve an increase or decrease in the SEI thickness during cycling, or the initial reduction products may react further with species in the electrolyte to form other compounds. In particular, the presence of trace moisture may lead to the formation of LiOH or Li_2O or the reaction with alkyl carbonates to form Li_2CO_3. Furthermore, the moisture may react with $LiPF_6$ to form HF, which reacts with carbonates to form LiF.[35] The reaction of carbonates with HF has been reported to occur based upon ex situ studies of $LiPF_6$/EC/DEC electrolytes.[36,37] These products may form to some extent during the initial stage of SEI formation, but it has also been shown that carbonates initially formed on the electrode may gradually be partly replaced by other lithium salts.[37] Therefore, the change in SLD of the pore is likely related to an increasingly dominant contribution of lithium salts with a lower SLD, such as Li_2O, LiOH, or LiF. Each of these salts has a SLD below that of $(CH_2OCO_2Li)_2$ and Li_2CO_3 (Figure 4) and will therefore increase the contrast with the carbon framework upon formation in Stage IIIa. A similar chemistry should occur in all cells. Due to the increasing moisture content of the cells with increasing deuteration level, it may be expected that the fraction of these products in the SEI will increase with deuteration level. In the 50%, 75%, and 100% cells, there would be no change in trend visible at the beginning of Stage III, as the trend of increasing peak intensity was present already in

dx.doi.org/10.1021/jp3012393 | J. Phys. Chem. C 2012, 116, 7701−7711

Stage II. The SANS data are consistent with an increasing fraction of lower SLD lithium salt forming due to reaction with an initial carbonate component of the SEI.

Stage IV: Charging. The final stage of the first full cycle of each cell is the charging stage in which lithium is removed from the carbon framework. Data have been obtained for the nondeuterated, 50%D, and 100%D cells (Figure 3) and show that in each case there is a large increase in the peak intensity during charging (~20% to 30% increase). This increase in peak intensity may be due to either a decrease in the SLD of the pore, an increase in the SLD of the framework, or a combination of the two effects. It has been reported that a change in the thickness of the SEI may occur during cycling, such that the SEI is thinner at high potentials (delithiated carbon) and thicker at low potentials (lithiated carbon).[38] On this basis, it is probable that changes in the thickness of the SEI make some contribution to the change in contrast during charging, though this cannot be directly confirmed from the available data. However, there is a clear decrease in the pore−pore spacing during charging (~0.5 Å); the associated volume decrease is a clear indication of the expected delithiation of the carbon framework. The delithiation is expected to increase the SLD of the carbon framework relative to the pore, as observed in the data.

The results of these studies are illustrated schematically in Figure 5 for the cell containing nondeuterated electrolyte. Trends in the contrast are shown in the middle of the figure and are qualitatively consistent with changes in the average SLD of the pore and framework during in situ cycling. The trends in peak intensity and pore−pore spacing can be well understood in terms of lithium adsorption/intercalation into the pore and framework and SEI formation and evolution.

4. SUMMARY AND CONCLUSIONS

A summary of the major results from this in situ SANS study of SEI formation and lithiation in mesoporous hard carbon includes:

(1) The formation of an SEI layer in the pores of the carbon framework has been observed for all cells. Furthermore, a change in the composition of the SEI layer during discharge is found to occur. The changes in contrast are consistent with the initial formation of Li_2CO_3 and/or $(CH_2OCO_2Li)_2$, followed by an increasing concentration of other low SLD salts such as Li_2O, LiOH, or LiF.

(2) Lithium insertion and removal from the carbon framework cannot account for the observed data in the absence of SEI formation.

(3) An increase in contrast between carbon framework and pore, in conjunction with an increase in pore−pore separation, occurs for all cells during the initial stage of discharge. These observations are consistent with an increase in the concentration of solvated lithium species near the carbon surface via adsorption/intercalation of lithium species. Further work is needed to confirm this hypothesis.

(4) Lithium insertion occurs at lower potential and becomes the dominant scattering process, as evidenced by a decrease in peak intensity and increase in pore−pore separation at low voltages.

(5) During charging, the decrease in pore−pore separation and increase in peak intensities indicate that the process of lithium removal from carbon has been observed.

Though there has been increasing interest in observing the formation of the SEI layer in situ, there are few approaches currently available. X-ray scattering and neutron scattering have been applied to the in situ studies of batteries but have not proved capable of observing the weak scattering from the thin, mixed phase SEI layer that typically forms on an electrode. Here we have demonstrated an approach that takes advantage of the contrast available in neutron scattering to observe directly the formation of the SEI layer in situ. These results will be extended to evaluate the thickness and quality of SEI layer formation, further evaluate the chemical changes occurring during initial and repeated cycling at both room temperature and elevated temperatures, and study other ordered mesoporous electrode materials.

■ ASSOCIATED CONTENT

Supporting Information

(1) Detailed summary of the protocol used for in situ cycling of half-cells on the EQ-SANS instrument. (2) Table of SLD values for various components (electrolyte, SEI components, carbon framework) contributing to scattering at the carbon electrode. (3) Figure providing an example of a fit to data collected on EQ-SANS for the nondeuterated half-cell prior to discharge. This material is available free of charge via the Internet at http://pubs.acs.org.

■ AUTHOR INFORMATION

Corresponding Author

*E-mail: bridgesca@ornl.gov.

Notes

The authors declare no competing financial interest.

■ ACKNOWLEDGMENTS

Research at ORNL was sponsored by the Materials Sciences and Engineering Division, Office of Basic Energy Sciences, U. S. Department of Energy. We acknowledge Carrie Gao for assistance with data collection at the Spallation Neutron Source (SNS). SAXS data to test the quality of mesoporous carbon samples were collected at the Center for Nanophase Materials Sciences (CNMS). Research at both SNS and CNMS was sponsored by the Scientific User Facilities Division, Office of Basic Energy Sciences, U.S. Department of Energy.

■ REFERENCES

(1) Buiel, E.; Dahn, J. R. *Electrochim. Acta* **1999**, *45*, 121.
(2) Aurbach, D.; Eineli, Y.; Chusid, O.; Carmeli, Y.; Babai, M.; Yamin, H. *J. Electrochem. Soc.* **1994**, *141*, 603.
(3) Aurbach, D.; Einely, Y.; Zaban, A. *J. Electrochem. Soc.* **1994**, *141*, L1.
(4) Zheng, T.; Liu, Y. H.; Fuller, E. W.; Tseng, S.; Vonsacken, U.; Dahn, J. R. *J. Electrochem. Soc.* **1995**, *142*, 2581.
(5) Zhou, H. S.; Zhu, S. M.; Hibino, M.; Honma, I.; Ichihara, M. *Adv. Mater.* **2003**, *15*, 2107.
(6) Guo, B.; Wang, X.; Fulvio, P. F.; Chi, M.; Mahurin, S. M.; Sun, X.-G.; Dai, S. *Adv. Mater.* **2011**, *23*, 4661.
(7) Su, D. S.; Schlogl, R. *ChemSusChem* **2010**, *3*, 136.
(8) Sato, K.; Noguchi, M.; Demachi, A.; Oki, N.; Endo, M. *Science* **1994**, *264*, 556.
(9) Xu, K. *Chem. Rev.* **2004**, *104*, 4303.
(10) Verma, P.; Maire, P.; Novak, P. *Electrochim. Acta* **2010**, *55*, 6332.
(11) Nagao, M.; Pitteloud, C.; Kamiyama, T.; Otomo, T.; Itoh, K.; Fukunaga, T.; Tatsumi, K.; Kanno, R. *J. Electrochem. Soc.* **2006**, *153*, A914.
(12) Stevens, D. A.; Dahn, J. R. *J. Electrochem. Soc.* **2001**, *148*, A803.

(13) Mamun, S. M.; Herstedt, M.; Oikawa, K.; Gustafsson, T.; Otomo, T.; Furusaka, M.; Kamiyama, T.; Sakaebe, H.; Edstrom, K. *Appl. Phys. A: Mater. Sci. Process.* **2002**, *74*, S1028.
(14) Amalraj, S. F.; Aurbach, D. J. *Solid State Electrochem.* **2011**, *15*, 877.
(15) Aurbach, D.; Levi, M. D.; Levi, E.; Schechter, A. *Proc. Symp. Batteries Portable Appl. Electr. Vehicles* **1997**, *97*, 953.
(16) Liang, C. D.; Li, Z. J.; Dai, S. *Angew. Chem., Int. Ed.* **2008**, *47*, 3696.
(17) Wang, X. Q.; Liang, C. D.; Dai, S *Langmuir* **2008**, *24*, 7500.
(18) Zhao, J. K.; Gao, C. Y.; Liu, D. *J. Appl. Crystallogr.* **2010**, *43*, 1068.
(19) Zhao, J. K. *Nucl. Instrum. Methods A* **2011**, *647*, 107.
(20) Zhao, J. K. *J. Appl. Crystallogr.* **2011**, *44*, 1277.
(21) Wong, P. Z.; Bray, A. J. *Phys. Rev. Lett.* **1988**, *60*, 1344.
(22) Debye, P.; Bueche, A. M. *J. Appl. Phys.* **1949**, *20*, 518.
(23) Debye, P.; Anderson, H. R.; Brumberger, H. *J. Appl. Phys.* **1957**, *28*, 679.
(24) Zhang, X.; Kostecki, R.; Richardson, T. J.; Pugh, J. K.; Ross, J. P. N. *J. Electrochem. Soc.* **2001**, *148*, A1341.
(25) Xu, K.; Cresce, A. v. *J. Mater. Chem.* **2011**, *21*, 9849.
(26) Besenhard, J. O.; Winter, M.; Yang, J.; Biberacher, W. *J. Power Sources* **1993**, *54*, 228.
(27) Xu, K.; Cresce, A. v.; Lee, U. *Langmuir* **2010**, *26*, 11538.
(28) Dresselhaus, M. S.; Dresselhaus, G. *Adv. Phys.* **2002**, *51*, 1.
(29) Yazami, R.; Deschamps, M. *J. Power Sources* **1995**, *54*, 411.
(30) Deschamps, M.; Yazami, R. *J. Power Sources* **1997**, *68*, 236.
(31) Takami, N.; Satoh, A.; Oguchi, M.; Sasaki, H.; Ohsaki, T. *J. Power Sources* **1997**, *68*, 283.
(32) Mabuchi, A.; Tokumitsu, K.; Fujimoto, H.; Kasuh, T. *J. Electrochem. Soc.* **1995**, *142*, 1041.
(33) Zheng, T.; Xing, W.; Dahn, J. R. *Carbon* **1996**, *34*, 1501.
(34) Zheng, T.; Gozdz, A. S.; Amatucci, G. G. *J. Electrochem. Soc.* **1999**, *146*, 4014.
(35) Aurbach, D. *J. Power Sources* **2000**, *89*, 206.
(36) Eineli, Y.; Markovsky, B.; Aurbach, D.; Carmeli, Y.; Yamin, H.; Luski, S. *Electrochim. Acta* **1994**, *39*, 2559.
(37) Aurbach, D.; Eineli, Y.; Markovsky, B.; Zaban, A.; Luski, S.; Carmeli, Y.; Yamin, H. *J. Electrochem. Soc.* **1995**, *142*, 2882.
(38) Edstrom, K.; Bryngelsson, H.; Stjerndahl, M.; Gustafsson, T. *J. Power Sources* **2007**, *174*, 970.